Dyes and Pigments 91 (2011) 286–293

Contents lists available at ScienceDirect

Dyes and Pigments

journal homepage: www.elsevier.com/locate/dyepig

High-temperature thermal and X-ray diffraction studies, and room-temperature spectroscopic investigation of some inorganic pigments

A.V. Knyazev [a,*], M. Mączka [b], E.N. Bulanov [a], M. Ptak [b], S.S. Belopolskaya [a]

[a] Nizhny Novgorod State University, Gagarin Prospekt 23/2, 603950 Nizhny Novgorod, Russia
[b] Institute of Low Temperature and Structure Research, Polish Academy of Sciences, P.O. Box 1410, 50-950 Wroclaw, Poland

ARTICLE INFO

Article history:
Received 18 February 2011
Received in revised form
11 May 2011
Accepted 17 May 2011
Available online 27 May 2011

Keywords:
Apatite
Spinel
Polymorphic transition
Thermal expansion
IR and Raman spectroscopy
Diffuse reflectance spectra

ABSTRACT

Inorganic Cr- and Mn-containing pigments of different structural types were investigated by high-temperature and spectroscopic methods. The differential scanning calorimetry in the temperature interval 298–1723 K was applied to measure temperatures of phase transition and melting of the studied compounds. High-temperature X-ray diffraction in the range 298–1173 K was used for the determination of the thermal expansion coefficients for the first time. Factor group analysis was used to predict general vibration modes of pigments and determine the activity of these vibrations in Raman and IR spectra, the Assignment of bands in Raman, IR and diffuse reflectance spectra was undertaken.

1. Introduction

Compounds with the general formula $M^{II}_5(A^VO_4)_3L$ (M^{II} = Ca, Sr, Ba, Cd, Pb; A^V = P, As, V, Mn, Cr; L = OH, F, Cl, Br, I) are subjects of interest to both geo- and bio-chemistry and each of them may be characterized as appetites. All of them can be referred to apatite class. These compounds are prospective materials for many technological applications. In particular, they can be used as a matrix for waste forms due to their isomorphic capacity, as inorganic pigments or they can be the building block of biocompatible and luminescent materials [1–4]. Apatite-type lanthanum silicates and germanates have also received a lot of interest as materials for solid oxide fuel cells [5–7]. Most of the individual compounds of the aforementioned general formula and solid solutions are based on them known as natural minerals, such as apatite $Ca_5(PO_4)_3F$, hydroxyapatite $Ca_5(PO_4)_3OH$, pyromorphite $Pb_5(PO_4)_3Cl$, endlichite $Pb_5(PO_4)_3F_xCl_{1-x}$ [8]. The science and technology community are interested in the exploration and application of such complexes.

Apatite compounds are structurally built of discrete AO_4 tetrahedra linked to one another by M^{II}-polyhedra, which form joint layers (Fig. 1). Apatite-type structures typically offer two crystallographic positions for cations differing in coordination number and local symmetry. The atoms occupying the first positions 4f form polyhedra shaped as three-capped trigonal prisms MO_9 having symmetry C3 whose columns run along the threefold axis. The coordination number (CN) of lead atoms occupying the second position depends on the type of ligand L: CN = 7 when L = F (distorted pentagonal bipyramids MO_6F), whereas CN = 8 when L = Cl (distorted two-capped trigonal prisms MO_6Cl_2). In consequence of differences of halogen positions, chlorine atoms occupy positions between layers formed by AO_4 tetrahedra, whereas fluorine atoms occupies positions within the layers (Fig. 1a) [9,10].

$CoCr_2O_4$ has a spinel structure and it crystallizes in a cubic space group Fd3m. Co atoms are located in tetrahedral positions 8a, while Cr atoms are located in octahedral positions 16d. O atoms of 32e position form a compact layer (Fig. 1b) [11].

The structure of Pb_2CrO_5 is built by distorted monocapped trigonal prisms connected to each other by edges to form endless hexahedral "rods" which are parallel to crystallographic axis *b*. These "rods" are joined by edges and tops of CrO_4 tetrahedra (Fig. 1) [12].

The structure of $K_2Ba(CrO_4)_2$ has yet to be solved: there are only space group and unit-cell parameters in XRD databases [13].

Compounds with the apatite structure, which are the subject of this study, i.e. $Ca_5(CrO_4)_3Cl$, $Sr_5(CrO_4)_3F$, $Ba_5(MnO_4)_3F$ and $Ba_5(MnO_4)_3Cl$, contain manganese (V) and chromium (V) in their composition. There

* Corresponding author.
E-mail address: knyazevav@gmail.com (A.V. Knyazev).

0143-7208/$ – see front matter © 2011 Elsevier Ltd. All rights reserved.
doi:10.1016/j.dyepig.2011.05.018

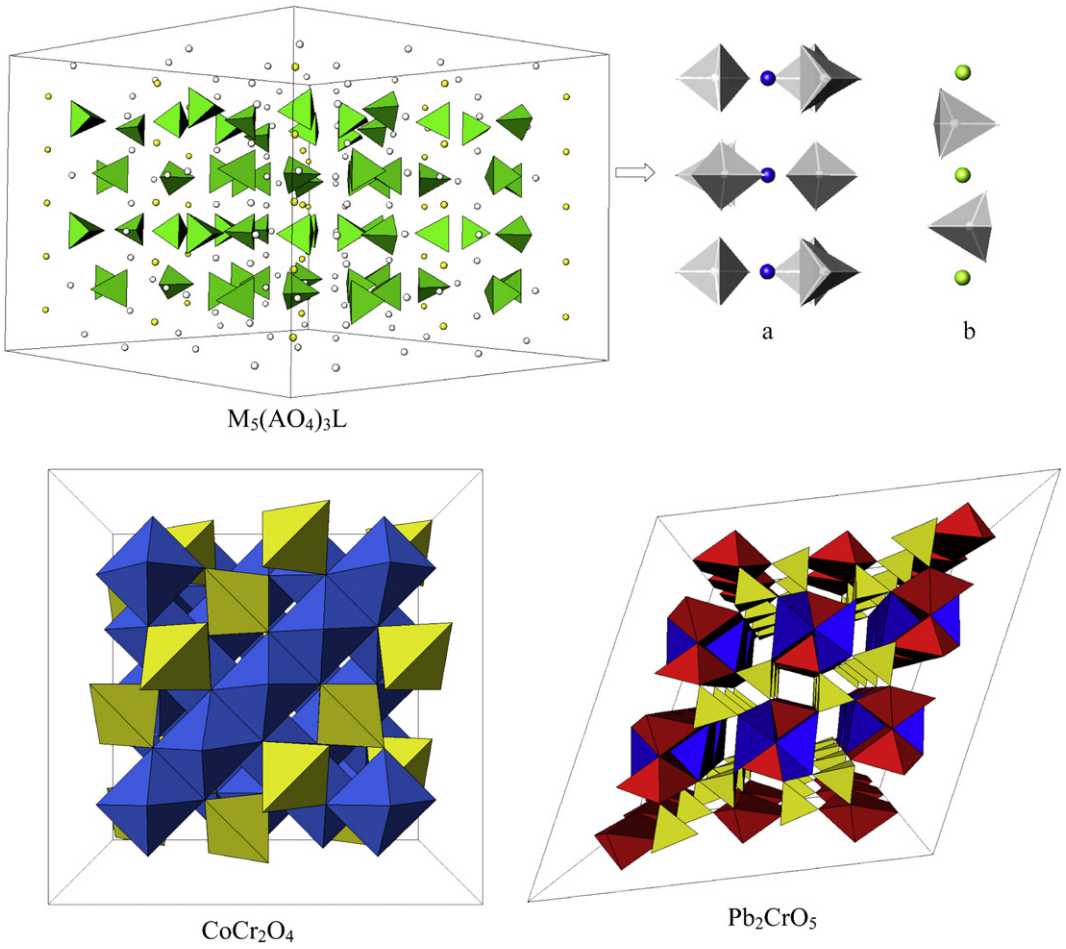

Fig. 1. Structure fragments of the studied compounds. For apatite structure different positions of halogen (L) are shown: $Sr_5(CrO_4)_3F$ (a) and $Ba_5(MnO_4)_3Cl$ (b) (blue spheres are F atoms, green spheres – Cl atoms). (For interpretation of the references to colour in this figure legend, the reader is referred to the web version of this article.)

are only a few publications dedicated to phases containing d-elements with uncommon oxidation state [9,14,15]. This dearth of information encouraged us to study such representatives of apatite class. Compounds of chromium (III) and chromium (VI) can also be used as pigments. In particular, we report in this work results for Pb_2CrO_5, $K_2Ba(CrO_4)_2$, and $CoCr_2O_4$ as potential pigments. The physicochemical properties of the aforementioned above Cr- and Mn-containing pigments were studied by X-ray diffraction method, including high-temperature experiments, IR, Raman and optical spectroscopy, and differential thermal analysis.

2. Experimental

2.1. Preparation of samples

Samples of the studied compounds were prepared by the solid-state reaction in accordance with the following equations. Final synthesis temperature is presented in brackets:

$$4.5CaCO_3 + 3CrO_3 + 0.5CaCl_2\cdot 2H_2O \rightarrow Ca_5(CrO_4)_3Cl + 4.5CO_2 + 0.75O_2 + H_2O\ (850\ ^\circ C)$$

$$4.5SrCO_3 + 3CrO_3 + 0.5SrF_2 \rightarrow Sr_5(CrO_4)_3F + 4.5CO_2 + 0.75O_2\ (800\ ^\circ C)$$

$$4.5BaCO_3 + 3MnO_2 + 0.5BaF_2 + 0.75O_2 \rightarrow Ba_5(MnO_4)_3F + 4.5CO_2\ (850\ ^\circ C)$$

$$4.5BaCO_3 + 3MnO_2 + 0.5BaCl_2\cdot 2H_2O + 0.75O_2 \rightarrow Ba_5(MnO_4)_3Cl + 4.5CO_2 + H_2O\ (750\ ^\circ C)$$

$$2Pb(NO_3)_2 + CrO_3 \rightarrow Pb_2CrO_5 + 4NO_2 + O_2\ (700\ ^\circ C)$$

$$BaCO_3 + K_2Cr_2O_7 \rightarrow K_2Ba(CrO_4)_2 + CO_2\ (700\ ^\circ C)$$

$$CoSO_4\cdot 7H_2O + Cr_2O_3 \rightarrow CoCr_2O_4 + SO_3 + 7H_2O\ (1100\ ^\circ C)$$

A reaction mixture of a set stoichiometry was placed in a porcelain crucible and calcined for 10 h with dispersion in an agate mortar every 2 h.

For all studied phases synthesis temperatures were reduced. Synthesis schemes were simplified in comparison with literature data by using one-step process [9–14].

2.2. Apparatus and measurement procedure

An atomic ratio of compounds under study was analyzed on a Shimadzu energy-dispersive roentgen fluorescent spectrometer EDX-900HS (from $_{11}$Na to $_{92}$U) with sensitive detector without liquid nitrogen.

The phase individuality of the synthesized compounds was monitored by X-ray diffraction. X-ray diffraction patterns were recorded on an XRD-6000 Shimadzu diffractometer (CuK_α radiation, geometry θ–2θ) in the 2θ range from 10° to 120° with scan increment of 0.02°.

High-temperature X-ray diffraction experiments in the range from 298 to 1173 K were carried out on the same diffractometer with increments of 0.02° ranging from 10° to 60° using an HA-1001 Shimadzu attachment.

Thermal experiments were carried out on a LABSYS Setaram differential scanning calorimeter at a heating rate of 10 K/min in an argon atmosphere. The samples were enclosed in platinum crucibles.

Polycrystalline infrared spectra were measured with a Biorad 575C FT-IR spectrometer in KBr suspension for the 1200–400 cm^{-1} region and in Nujol suspension for the 500–50 cm^{-1} region. Raman spectra of $K_2Ba(CrO_4)_2$ and Pb_2CrO_5 were measured using BRUKER 110/S spectrometer and 1064 nm line of a YAG:Nd^{3+} laser as an excitation source. Since the Raman spectra of $Ca_5(CrO_4)_3Cl$, $Sr_5(CrO_4)_3F$ and $CoCr_2O_4$ could not be recorded by the Bruker instrument due to strong luminescence background, spectra of these compounds were measured using Renishow spectrometer with confocal microscope and 830 nm laser line as an excitation source. Both IR and Raman spectra were recorded with a spectral resolution of 2 cm^{-1}. Unfortunately, Raman spectra of $Ba_5(MnO_4)_3F$ and $Ba_5(MnO_4)_3Cl$ could not be recorded neither with Bruker nor Renishow spectrometer due to a very strong luminescence background and, therefore, for these compounds only IR spectra have been measured.

Electron reflectance spectra were measured using a Cary 5E spectrophotometer with the Praying Mantis diffuse reflectance accessory.

3. Results and discussion

3.1. Differential scanning calorimetry

The joint application of the high-temperature X-ray diffraction and thermal analysis (TG–DTA) made it possible to establish some peculiarities of processes taking place in the compounds under investigation during heating. Fig. 2 represents DTA curves of the studied compounds. All of the compounds except of Pb_2CrO_5, decompose either by incongruent melting ($Sr_5(CrO_4)_3F$, $K_2Ba(CrO_4)_2$) or thermal decomposition below their melting point ($Ca_5(CrO_4)_3Cl$, $Ba_5(MnO_4)_3F$, $Ba_5(MnO_4)_3Cl$). For Pb_2CrO_5 congruent melting is typical (Table 1).

The DTA curve of $Ca_5(CrO_4)_3Cl$ exhibits several endothermic effects. The first peak at 907 K was attributed to a reversible polymorphic transition without change of the crystal system ("hexagonal-1" → "hexagonal-2"), which was confirmed by X-ray diffraction data. The second effect is connected with thermal decomposition of the phase. After the second effect the parent phase was not detected.

There are three endothermic peaks on the DTA curve of Pb_2CrO_5 below its melting point. These effects correspond to reversible polymorphic transitions.

There is only modelled melting point in literature for $CoCr_2O_4$; as a consequence of this high value this data could not be confirmed using our currently available equipment.

Melting and decomposition products, established by XRD analysis, were not identified due to the complexity of their composition and absence in the PDF4 and FindIt XRD databases.

The TG curve did not show any mass changes during the experiment, so it may be concluded that the stoichiometric composition of the system did not change.

3.2. High-temperature X-ray diffraction

High-temperature X-ray diffraction experiments were undertaken to assess the nature of the polymorphic transformation of $Ca_5(CrO_4)_3Cl$. It was found that the polymorphic transition doesn't lead to change of the unit-cell symmetry and it corresponds to an inter-conversion from one "hexagonal" to another "hexagonal" arrangement. As we reported earlier [17] presence of polymorphic transition in apatites, especially in lead-containing compounds, is typical. But in these cases the transition corresponds to a reduction of unit-cell symmetry in compliance with the conversion "hexagonal" to "monoclinic".

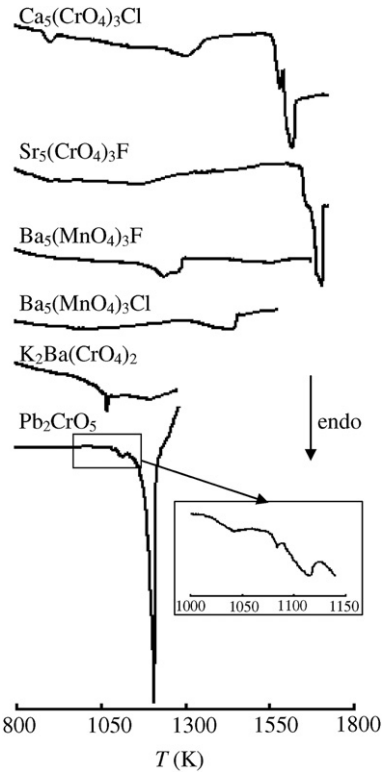

Fig. 2. DTA curves of the compounds under study.

The aforementioned difference can be explained based on the following assumptions. In both cases (Ca-containing and Pb-containing apatites) reduction of symmetry is observed, as opposed to literature data concerning the rise of the symmetry after polymorphic transition [18,19]. The symmetry reduction process promotes an increase of the apatites thermal stability. Because of higher polarizability of Pb atoms, lead-containing phases have much more possibilities to rebuild structure as compared with Ca-containing compounds. This feature explains why the reduction of unit-cell symmetry in Pb apatites is more appreciable than in Ca apatites.

High-temperature X-ray diffraction was used not only for studying phase transitions, but also for determining thermal

Table 1
Phase transition temperatures of the studied compounds.

Compound	T_{tr} (K)	T_d (K)	T_m (K)
$Ca_5(CrO_4)_3Cl$	907	1300	–
$Sr_5(CrO_4)_3F$	–	–	1705
$Ba_5(MnO_4)_3F$	–	1234	–
$Ba_5(MnO_4)_3Cl$	–	1436	–
$BaK_2(CrO_4)_2$		1064	
Pb_2CrO_5	1041 1083 1113		1206
$CoCr_2O_4$		2271 [16]	

expansion coefficients (Table 2). For solving this problem, $a = f(T)$ equations were fitted by either linear or quadratic functions and calculations were carried out using the DTC program [18]. At the polymorphic transformation temperature T_{tr} the temperature dependences of the unit-cell parameters and volume for $Ca_5(CrO_4)_3Cl$ show breaks (Fig. 3).

The data compiled in Table 2 show that all apatite compounds under study, regardless of the polymorph, have an anisotropy of thermal expansion, and these phases of the apatite family may be classified as strongly expanding compounds in terms of the classification system described in [19]. Fig. 4a shows thermal expansion diagrams for the studied apatites, which were built up in KTP program [18]. The value of thermal expansion coefficient in a given direction corresponds to length of radius-vector, which is traced from origin of coordinates to edge of figure of expansion.

It is remarkable that the preferred crystallographic direction upon expansion is the unit-cell parameter *a*, as opposed to the most of apatite phases [17]. This factor may be explained by the greater strength of interlayer interactions compared to chemical bonds in layers formed by AO_4 tetrahedra.

For $Ca_5(CrO_4)_3Cl$ at the polymorphic transition temperature the character of thermal expansion sharply changes due to a decrease of the unit-cell parameter *a* above this temperature. Hereupon we observed areas with negative thermal expansion on relevant diagram (Fig. 4a).

Compound $CoCr_2O_4$ (Fig. 4b) with a spinel structure has the least thermal expansion coefficients and the greatest thermal stability as compared with the other studied phases.

As opposed to the mentioned apatite compounds, in $K_2Ba(CrO_4)_2$ the tendency of isotropic thermal expansion is observed upon increase of temperature. At 973 K thermal expansion coefficients along the crystallographic axes *a* and *c* become equal.

Thermal expansion in the crystallographic plane *cb* of Pb_2CrO_5 is practically isotropic, whereas the thermal expansion coefficient

Table 2
Thermal expansion coefficients as functions of temperature for compounds under study.

Compound	$\alpha_i = (kT + m) \times 10^{-6}$ (K^{-1})		
	i	$k \times 10^2$	*m*
α-$Ca_5(CrO_4)_3Cl$	*a*	1.171	11.0
	c	1.024	1.9
	V	3.361	23.8
β-$Ca_5(CrO_4)_3Cl$	*a*	–	−4.7
	c	–	22.7
	V	–	13.2
$Sr_5(CrO_4)_3Cl$	*a*	0.877	8.8
	c	0.939	5.3
	V	2.698	22.9
$Ba_5(MnO_4)_3F$	*a*	1.557	3.9
	c	1.139	3.8
	V	4.247	11.6
$Ba_5(MnO_4)_3Cl$	*a*	1.695	5.8
	c	2.615	−1.0
	V	6.016	10.4
$K_2Ba(CrO_4)_2$	*a*	2.962	9.7
	c	3.840	1.1
	V	9.772	20.0
$CoCr_2O_4$	*a*	0.488	3.9
	V	1.486	11.5
Pb_2CrO_5	*a*	1.200	−1.7
	b	5.041	3.8
	c	4.636	6.9
	β	1.665	−8.5
	V	9.276	1.7

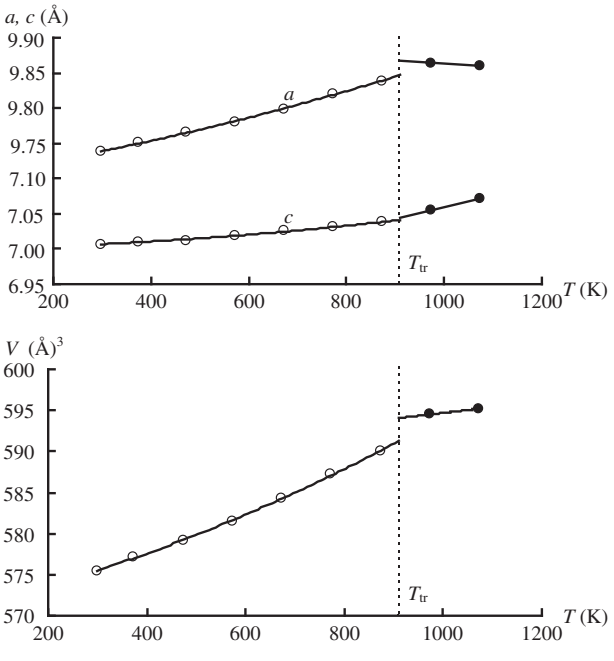

Fig. 3. Unit-cell parameters as a function of temperature for $Ca_5(CrO_4)_3Cl$.

along the crystallographic axis *a* is 5–10 times smaller than the coefficients along the *b* and *c* axes. Analyzing the *b*-angle change it may be concluded that at temperature > 773 K the *b*-angle begins to quickly tend to 120°. That is why it may be assumed that the phase transitions, which are observed in the compound, can be connected with a rising of the unit-cell symmetry from monoclinic to hexagonal.

3.3. IR and Raman studies

3.3.1. Apatite compounds

Factor group analysis of the hexagonal $Ca_5(CrO_4)_3Cl$ and $Ba_5(MnO_4)_3Cl$ apatites ($P6_3/m$, $Z = 2$) shows that the normal modes are distributed among $12A_g + 12E_{2g} + 8B_g + 8E_{1g} + 13B_u + 13E_{1u} + 9A_u + 9E_{2u}$ irreducible representations. For $Sr_5(CrO_4)_3F$ and $Ba_5(MnO_4)_3F$ the normal modes are distributed among $12A_g + 13E_{2g} + 9B_g + 8E_{1g} + 12B_u + 13E_{1u} + 9A_u + 8E_{2u}$ irreducible representations. The difference in the reproducible representations for the Cl- and F-apatites is due to the fact that Cl atoms occupy 2b sites and F atoms 2a sites in the $P6_3/m$ structure [9,10]. Since the A^V–O bonds (A^V = Cr, Mn) are much stronger than the M^{II}–O bonds (M^{II} = Ca, Sr, Ba), the crystal structure can be treated as composed of A^VO_4 tetrahedra, M^{II} ions and L ions (L = Cl, F). We may, therefore, subdivide the vibrational modes into symmetric stretching modes of A^VO_4 (ν_1: $A_g + E_{2g} + B_{1u} + E_{1u}$), asymmetric stretching modes of A^VO_4 (ν_3: $2A_g + 2E_{2g} + B_g + E_{1g} + 2B_{1u} + 2E_{1u} + A_u + E_{2u}$), symmetric bending modes of A^VO_4 (ν_2: $A_g + E_{2g} + B_g + E_{1g} + B_{1u} + E_{1u} + A_u + E_{2u}$), asymmetric bending modes of A^VO_4 (ν_4: $2A_g + 2E_{2g} + B_g + E_{1g} + 2B_{1u} + 2E_{1u} + A_u + E_{2u}$), translations of A^VO_4 (T: $2A_g + 2E_{2g} + B_g + E_{1g} + 2B_{1u} + 2E_{1u} + A_u + E_{2u}$), librations of A^VO_4 (L: $A_g + E_{2g} + 2B_g + 2E_{1g} + B_{1u} + E_{1u} + 2A_u + 2E_{2u}$), translations of M^{II} ions (T: $3A_g + 3E_{2g} + 2B_g + 2E_{1g} + 3B_{1u} + 3E_{1u} + 2A_u + 2E_{2u}$), and vibrations of Cl ($B_u + A_u + E_{2u} + E_{1u}$) or F ($B_g + A_u + E_{2g} + E_{1u}$) ions. From these modes, two modes should be classified as acoustic ($A_u + E_u$). The A_g, E_{1g} and E_{2g} modes are Raman active, A_u and E_{1u} modes are IR active, and B_g, B_u and E_{2u} modes are optically silent.

The recorded Raman spectra show the presence of a strong (weak) band at 829 (778) and 820 (789) cm^{-1} for $Ca_5(CrO_4)_3Cl$ and

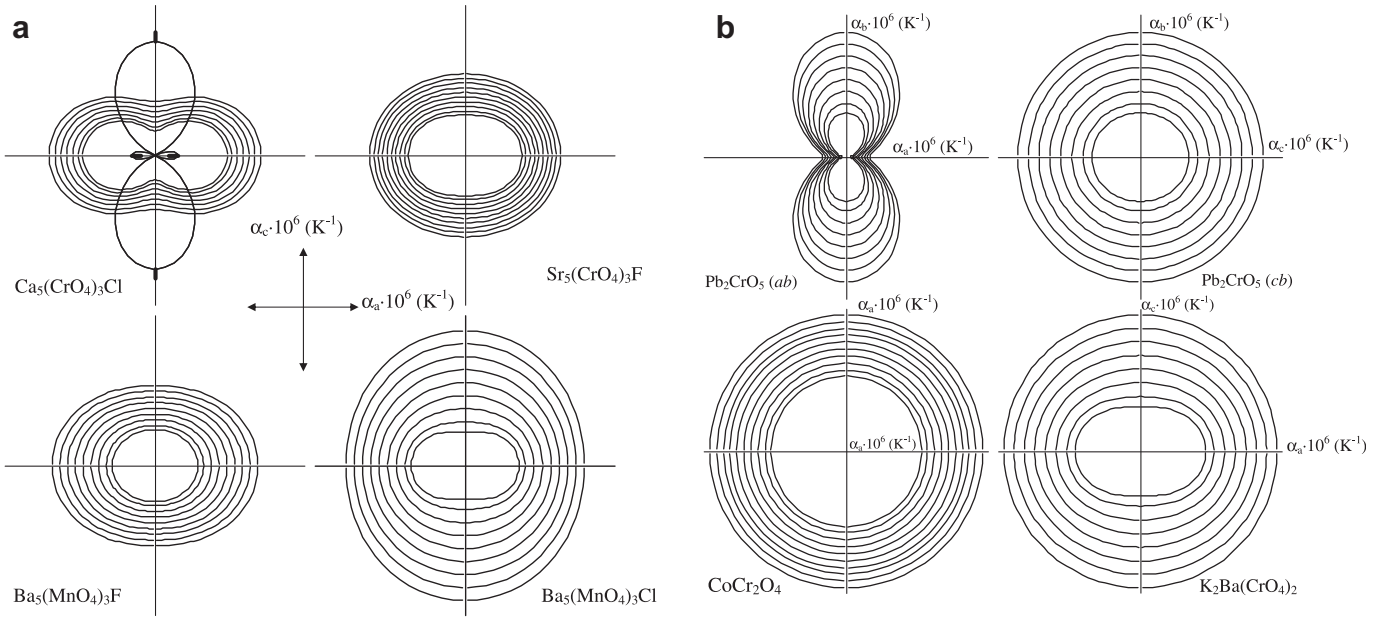

Fig. 4. Thermal expansion diagrams for the compounds under study. All apatite diagrams (a) are given in single scale $30 \times 30 \times 10^6$ (K^{-1}). For diagram of $Ca_5(CrO_4)_3Cl$ directions of expansion are shown by heavy strokes. Other diagrams (b) correspond to the following scales: $60 \times 60 \times 10^6$ (K^{-1}) (Pb_2CrO_5), $10 \times 10 \times 10^6$ (K^{-1}) ($CoCr_2O_4$), $40 \times 40 \times 10^6$ (K^{-1}) ($K_2Ba(CrO_4)_2$). Diagram for Pb_2CrO_5 is given in two crystallographic planes *ab* and *cb*.

$Sr_5(CrO_4)_3F$, respectively (see Fig. 5). According to the literature data the higher wavenumber band can be assigned to symmetric stretching mode and the lower wavenumber band to the asymmetric stretching mode of CrO_4^{3-} ions [20–22]. The corresponding bending modes give rise to a broad band in the 380–360 cm^{-1} range.

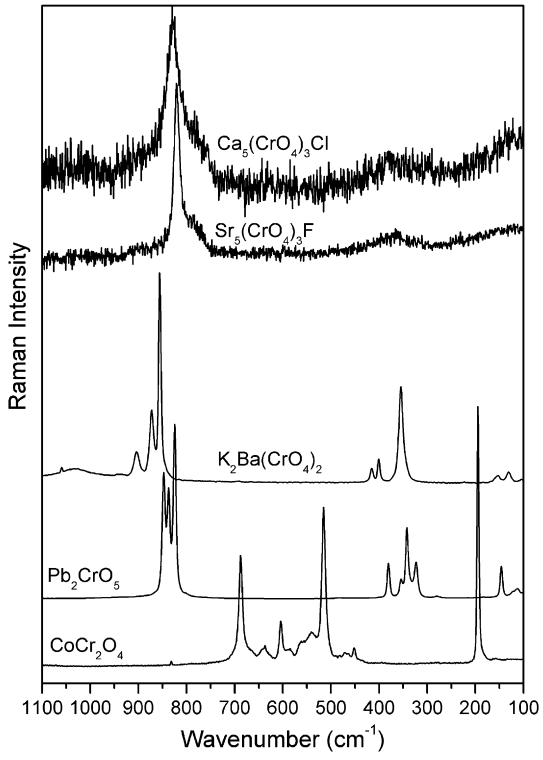

Fig. 5. Raman spectra of the studied compounds.

IR spectra of the studied apatites are more informative. Table 3 lists wavenumbers of all observed IR modes together with the proposed assignment based on comparison of our data with literature data for other apatite-type compounds. Results presented in Fig. 6 and Table 3 allow us to obtain a few conclusions. First, IR spectra of chromates show a number of weak bands above 860 cm^{-1} (see Table 3). According to the literature data stretching modes of CrO_4^{3-} ions are expected in the 770–870 cm^{-1} range [20–22]. We assign, therefore, all weak bands above 870 cm^{-1} for the Cr-apatites and above 860 cm^{-1} for $Ba_5(MnO_4)_3F$ to overtones and/or impurity phases (most likely CrO_4^{2-} and MnO_4^{2-} ions). Second, the obtained data show that stretching modes of CrO_4^{3-} ions are observed at higher wavenumbers (776–845 cm^{-1}) than the corresponding modes of the MnO_4^{3-} ions (751–793 cm^{-1}). This result is in agreement with the literature data, which showed lower values of the stretching modes for the manganese ions [20]. Third, the stretching modes of CrO_4^{3-} ions are observed in a broader wavenumber range than the corresponding modes of the MnO_4^{3-} ions (see above). This effect is also observed for other chromates and manganates [20–22]. Fourth, the IR bands in the stretching mode region are significantly narrower for $Sr_5(CrO_4)_3F$ when compared to $Ca_5(CrO_4)_3Cl$. A similar effect is also observed for the symmetric stretching mode in the Raman spectra. It is well known that apatites are usually somewhat non-stoichiometric [23]. Moreover, larger L anions (Cl, Br, I) may be displaced away from their special positions, especially if the *6h* sites are occupied by smaller cations [23]. We suppose, therefore, that large broadening of bands for $Ca_5(CrO_4)_3Cl$ may indicate significant non-stoichiometry of this compound and/or significant displacements of Ca^{2+} ions from the *6h* positions. Fifth, both IR and Raman bands are observed at lower wavenumbers for $Sr_5(CrO_4)_3F$ than for $Ca_5(CrO_4)_3Cl$. This effect is consistent with a larger lattice parameter for the first compound. Finally, whereas the IR spectra of $Ba_5(MnO_4)_3Cl$ and $Ba_5(MnO_4)_3F$ are very similar above 300 cm^{-1}, they show significant differences below 300 cm^{-1}. This effect is related to replacement of lighter F atoms by much heavier Cl atoms. For instance, the band observed at 267 cm^{-1} for $Ba_5(MnO_4)_3F$ is not

Table 3
IR wavenumbers for the studied apatites together with the proposed assignment. Sh, vw, w, m, s, vs denote shoulder, very weak, weak, medium, strong and very strong, respectively.

$Ca_5(CrO_4)_3Cl$	$Sr_5(CrO_4)_3F$	$Ba_5(MnO_4)_3F$	$Ba_5(MnO_4)_3Cl$	Assignment
940sh	940sh	–	–	Overtones and/
–	925vw	–	–	or impurity
912sh	913w	–	–	
–	904w	896vw	–	
–	884w	882vw	–	
–	875w	861vw	–	
845m	843s	793w	793w	Stretching modes
–	819s	783vw	782w	of AO_4
796s	776vs	751vs	754vs	
617w	–	–	–	Overtone
389m	378m	358m	363m	Bending modes
357m	346m	329m	330m	of AO_4
306m	297m	–	321m	
–	272sh	267m	–	Translations
				of F atoms
245m	205m	193sh	204w	Lattice modes
224w	–	178m	–	
202m	194s	162m	173m	
167w	161s	139m	150w	
–	–	–	131m	
–	120sh	–	102vw	
–	–	85vw	79vw	
78w	68w	61vw	61vw	

observed for $Ba_5(MnO_4)_3Cl$. Similar behaviour is observed for the 272 cm^{-1} band of $Sr_5(CrO_4)_3F$. We assign, therefore, this band to motions of the F ligand. The corresponding mode of Cl ligand is expected to shift towards lower wavenumbers due to the higher atomic mass of Cl. We suppose that vibrations of Cl ligand are coupled with translational modes of CrO_4^{3-} and MnO_4^{3-} ions, and contribute to modes observed below 200 cm^{-1}.

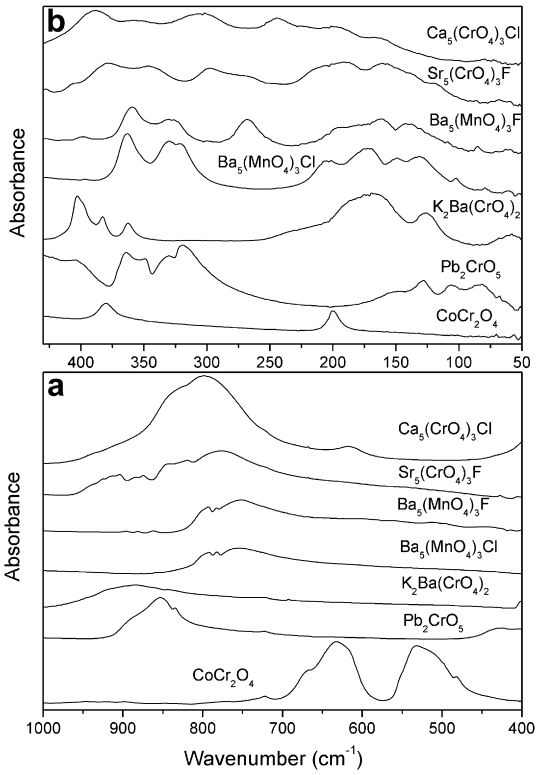

Fig. 6. (a) Mid-IR and (b) far-IR spectra of the studied compounds.

3.3.2. Pb_2CrO_5

The structure of Pb_2CrO_5 is monoclinic, C2/m (C_{2h}^3) [12]. It is built by distorted monocapped trigonal prisms connected to each other by edges to form endless hexahedral "rods" and CrO_4 tetrahedra (Fig. 1c). There are two crystallographically nonequivalent Pb atoms and one Cr atom occupying 4i sites of C_s symmetry [12]. Factor group analysis for the C2/m structure of Pb_2CrO_5 predicts $14A_g + 10B_g + 9A_u + 15B_u$ Brillouin zone centre modes. These modes can be subdivided into the vibrational modes into symmetric stretching modes of CrO_4 (ν_1: $A_g + B_u$), asymmetric stretching modes of CrO_4 (ν_3: $2A_g + B_g + A_u + 2B_u$), symmetric bending modes of CrO_4 (ν_2: $A_g + B_g + A_u + B_u$), asymmetric bending modes of CrO_4 (ν_4: $2A_g + B_g + A_u + 2B_u$), translations of CrO_4 (T: $2A_g + B_g + A_u + 2B_u$), librations of CrO_4 (L: $A_g + 2B_g + 2A_u + B_u$), translations of Pb^{2+} ions (T: $4A_g + 2B_g + 2A_u + 4B_u$) and vibrations involving the O(4), which form chemical bonds only with lead ions ($A_g + 2B_g + A_u + 2B_u$). From these modes, two modes should be classified as acoustic ($A_u + 2B_u$). The A_g and B_g modes are Raman active, and A_u and B_u modes are IR active.

The Raman (IR) spectrum shows bands at 847, 838 and 825 cm^{-1} (889, 854 and 834 cm^{-1}), which can be assigned to stretching modes of the CrO_4^{2-} ions [20,24,25]. The 825 cm^{-1} mode, which is not observed in the IR spectrum, can be assigned to a symmetric stretching mode, and the remaining modes to asymmetric stretching modes. In the bending mode region Raman-active (IR-active) modes are observed at 381, 355, 342, 324 and 279 cm^{-1} (430, 407, 364, 350, 331 and 319 cm^{-1}). According to the factor group analysis five bands are expected both in Raman and IR spectra for bending modes of CrO_4^{2-} ions. Observation of 6 bands in the IR spectrum can be most likely attributed to additional contribution from the Pb–O(4) stretching mode. In the low wavenumber region Raman (IR) bands are observed at 146, 122, 113 and 103 cm^{-1} (150, 128, 106 and 84 cm^{-1}). Former studies of lead apatites showed that translations of Pb^{2+} ions were observed near 60 cm^{-1} [1]. In our case, these motions contribute most likely contribute to the band observed at 84 cm^{-1}. The remaining bands in this region can be attributed to translations and vibrations of CrO_4^{2-} ions.

3.3.3. $K_2Ba(CrO_4)_2$

The structure of $K_2Ba(CrO_4)_2$ was not solved and therefore it is not possible to calculate the number of expected Raman and IR modes. Nevertheless, both Raman and IR spectra show very clearly two groups of bands, which can be assigned to stretching and

Table 4
Raman and IR wavenumbers for Pb_2CrO_5 and $K_2Ba(CrO_4)_2$ together with the proposed assignment b means broad.

Pb_2CrO_5		$K_2Ba(CrO_4)_2$		Assignment
Raman	IR	Raman	IR	
847s	889m	904w	917sh	Stretching modes of CrO_4
838m	854s	873m	884vs	
825s	834w	856s	843vw	
–	–	–	722vw	Overtones?
–	–	–	693vw	Overtones?
388m	430m	415w	403m	Bending modes of CrO_4 and Pb–O
355w	407w	401w	383w	Stretching (for the lead compound)
342m	364m	355s	363w	
324w	350m	344sh	–	
–	331m	–	–	
–	319m	–	–	
146m	150w	–	230m,b	Lattice modes
122sh	128m	–	184sh	
113w	106m	154w	170m	
103sh	84m	131w	126m	
–	–	104w	58w	

bending modes of CrO_4^{2-} ions (Figs. 5 and 6, Table 4). These bands are observed at higher wavenumbers, when compared to Pb_2CrO_5. This result indicates shorter Cr–O bonds in this compound. Lattice modes are also observed at higher wavenumbers, when compared to Pb_2CrO_5. This result can mainly be attributed to presence of lighter ions (K^+, Ba^{2+}) in this structure and thus higher wavenumbers of the corresponding translational modes, when compared to heavy Pb^{2+} ions.

3.3.4. $CoCr_2O_4$

$CoCr_2O_4$ crystallizes in the spinel type structure. According to the factor group analysis, four IR ($4F_{1u}$) and five Raman modes (A_{1g}, E_g, 3 F_{2g}) should be observed for this compound [26,27]. Our Raman (IR) spectrum shows bands at 688m, 639w, 605w, 586w, 560w, 541w, 516s, 451vw and 195vs cm^{-1} (721w, 666vw, 632vs, 532vs, 482vw, 380m and 201m cm^{-1}). The position of the IR bands at 380 and 201 cm^{-1} are in very good agreement with lattice dynamic calculations and previous experimental studies on single crystals [26,27]. However, the two most intense bands are observed at higher wavenumbers in our study of polycrystalline samples (632 and 532 cm^{-1}) than the transverse optical (TO) values estimated from studies performed on single crystal (609 and 491 cm^{-1} [26]) or lattice dynamics calculations (603 and 488 cm^{-1} [27]). This effect is due to a shift of IR bands towards higher wavenumbers, i.e. towards the longitudinal optical (LO) values, and it is often observed for polycrystalline spectra of ionic crystals [28]. In the case of Raman spectra, the 688m, 516s, 451vw and 195vs cm^{-1} are in good agreement with experimental (687 and 457 cm^{-1} [26]) or calculated data (692, 523, 454 and 192 cm^{-1} [27]). The fifth mode was calculated at 382 cm^{-1} [27] but our Raman spectrum does not show any band near 380 cm^{-1}. We suppose that this band is either too weak to be observed in our experiment or has higher wavenumber. Our Raman and IR spectra shows also a number of weak bands in the 450–650 cm^{-1} range and at 721, 666 and 482 cm^{-1}, respectively, which can be most likely attributed to some impurities and/or overtones.

3.4. Diffuse reflectance spectra

The spectra of Pb_2CrO_5 and $K_2Ba(CrO_4)_2$ exhibit a strong increase of absorption at wavelengths lower than 650 and 500 nm, respectively (Fig. 7). The CrO_4^{2-} group is typical example of the closed shell molecular complex of tetrahedral coordination. Therefore, the only absorption transitions can be via the charge transfer (CT) from ligands to the central ions. It has been shown that the ground state absorption should have two CT bands: one is often observed at 360 nm and the other one is often immersed in the band-to-band absorption edge [29]. The spectrum of $K_2Ba(CrO_4)_2$ shows maxima at 402, 338, 293 and 265 nm, which can be attributed to CT bands of the CrO_4^{2-} group. The presence of four components can be most likely attributed to presence of different sites occupied by CrO_4^{2-} ions in the $K_2Ba(CrO_4)_2$ structure. The spectrum of Pb_2CrO_5 shows two maxima at about 500 and 340 nm. The maximum at 340 nm can be attributed to CT transition within the CrO_4^{2-} group. The origin of the second maximum at 500 nm is less clear. One of the possible explanation is that this maximum corresponds to Cr^{5+} ions, which may appear in the Pb_2CrO_5 sample due to defects, i.e. oxygen vacancies.

The spectrum of $CoCr_2O_4$ exhibits maxima at 267, 342, 420, 580, 612, 652, 1360, 1392, 1547 and 1618 nm. The bands in the 400–700 nm range are characteristic for $^4A_{2g} \rightarrow {}^4T_{2g}$, $^4A_{2g} \rightarrow {}^4T_{1g}$ and $^4A_{2g} \rightarrow {}^2E_g$ absorptions of the octahedrally coordinated Cr^{3+} ions and $^4A_2$ (^4F) $\rightarrow {}^4T_1$ (^4P) absorptions of the Co^{2+} ions [29–31]. The bands below 400 nm can be most likely attributed to CT transitions and the four bands in the 1360–1618 nm range arise due to $^4A_2$ (^4F) $\rightarrow {}^4T_1$ (^4F) transitions of the Co^{2+} ions [30,31]. It is worth noting that former studies of Co^{2+} ions in $MgAl_2Se_4$ and $CaAl_2Se_4$ also showed four bands due to $^4A_2$ (^4F) $\rightarrow {}^4T_1$ (^4F) transitions of the Co^{2+} ion in T_d symmetry [31]. However, these bands were observed at significantly higher wavelength (1500–2000 nm) than in $CoCr_2O_4$. This result indicates that Co^{2+} ions in $CoCr_2O_4$ are located at sites with significantly higher crystal field strength, when compared to $MgAl_2Se_4$ and $CaAl_2Se_4$.

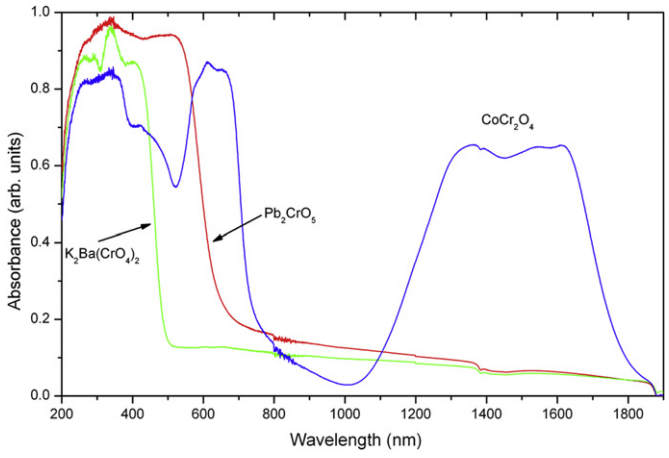

Fig. 7. Diffuse reflectance spectra of Pb_2CrO_5, $K_2Ba(CrO_4)_2$ and $CoCr_2O_4$.

4. Conclusions

Thus inorganic Cr- and Mn-containing pigments of different structural types were investigated by high-temperature and spectroscopic methods. The differential scanning calorimetry in the temperature interval 298–1723 K was applied to measure temperatures of phase transition and melting of $Ca_5(CrO_4)_3Cl$, $Sr_5(CrO_4)_3F$, $Ba_5(MnO_4)_3F$, $Ba_5(MnO_4)_3Cl$, $K_2Ba(CrO_4)_2$, Pb_2CrO_5, $CoCr_2O_4$. Thermal expansion coefficients of all studied compounds were determined by the high-temperature X-ray diffraction in the range 298–1173 K. A detailed assignment of bands in Raman, IR and diffuse reflectance spectra was made.

Acknowledgements

The work was financially supported by the federal goal-oriented program “Scientific and scientific-pedagogical personnel of innovative Russia” (grant НК-540П).

References

[1] Zhang M, Maddrell ER, Abraitis PK, Salje EKH. Impact of leach on lead vanadoiodoapatite [$Pb_5(VO_4)_3I$]: an infrared and Raman spectroscopic study. Mat Sci Eng B 2007;137:149–55.
[2] Best SM, Porter AE, Thian ES, Hyang J. Bioceramics: past, present and for the future. J Eur Ceram Soc 2008;28:1319–27.
[3] Zhang J, Liang H, Yu R, Yuan H, Su Q. Luminescence of Ce^{3+}-activated chalcogenide apatites $Ca_{10}(PO_4)_6Y$ (Y = S, Se). Mat Chem Phys 2009;114:242–6.
[4] Knyazev AV, Chernorukov NG, Bulanov EN. High-temperature investigation of compounds with composition $Ba_5(A^VO_4)_3Cl$ (AV = P, V, Mn). Vestnik of NNSU 2010;6:87–92 [in Russian].
[5] Rodriguez-Reyna E, Fuentes AF, Maczka M, Hanuza J, Boulahya K, Amador U. Structural, microstructural and vibrational characterization of apatite-type lanthanum silicates prepared by mechanical milling. J Solid State Chem 2006;179:522–31.
[6] Rodriguez-Reyna E, Fuentes AF, Maczka M, Hanuza J, Boulahya K, Amador U. Facile synthesis, characterization and electrical properties of apatite-type lanthanum germinates. Sol State Sci 2006;8:168–77.

[7] Kendrick E, Islam MS, Slater PR. Developing apatites for solid oxide fuel cells: insight into structural, transport and doping properties. J Mater Chem 2007; 17:3104–11.
[8] Betekhtin AG. The course of mineralogy [Gosudarstvennoe izdatel'stvo geologicheskoi literatury]. Moscow; 1951 [in Russian].
[9] Reinen D, Lachwa H, Allmann R. EPR- und ligandenfeldspektroskopische Untersuchungen an Mn(V)-haltigen Apatiten sowie die Struktur von $Ba_5(MnO_4)_3Cl$. Z Anorg Allg Chem 1986;542:71–88.
[10] Herdtweck E. Structure of decastrontium hexachromate (V) difluoride. Acta Cryst C 1991;47:1711–2.
[11] Pernet M, Quezel G, Coing-Boyat J, Bertaut EF. Structures magnetiques des chromates de cobalt et de nickel. Bull Soc Franc Mineral Cristallogr 1969;92:264–73.
[12] Morita S, Toda K. Determination of the crystal structure of Pb_2CrO_5. J Appl Phys 1984;55:2733–7.
[13] Schwarz H. Doppelverbindungen vom Typ $Me(Me^{II}(X^{VI}O_4))_2$ mit der Struktur von $Sr_3(PO_4)_2$. III. Chromate. Z Anorg Allg Chem 1966;345:230–45.
[14] Fielder DA, Albering JH, Besenhard JO. Characterization of strontium and barium manganates by abrasive stripping voltammetry. J Solid State Electrochem 1998;2:413–9.
[15] Reinen D, Albrecht C, Kaschuba U. EPR- und ligandenfeldspektroskopische Untersuchungen an Chrom(V)-haltigen Apatiten und Spodiositen. Z Anorg Allg Chem 1990;584:71–86.
[16] Ostby J, Chen M. Thermodynamic assessment of the CoO_x–$CrO_{1.5}$ system. J Alloys Compd 2009;485:427–34.
[17] Chernorukov NG, Knyazev AV, Bulanov EN. Phase transitions and thermal expansion of apatite-structured compounds. Inorg Mater 2011;47:172–7 [in Russian].
[18] Belousov RI, Filatov SK. Algorithm for calculating the thermal expansion tensor and constructing the thermal expansion diagram for crystals. Glass Phys Chem 2007;33:271–5 [in Russian].
[19] Filatov SK. High-temperature crystal chemistry. Theory, methods, and results. Leningrad: Nedra; 1990 [in Russian].
[20] Nakamoto K. Infrared and Raman spectra of inorganic and coordination compounds. 6th ed. John Wiley & Sons; 2009.
[21] Long YW, Yang LX, Yu Y, Li FY, Lu YX, Yu RC, et al. High-pressure Raman scattering study on zircon-to scheelite-type structural phase transitions of $RCrO_4$. J Appl Phys 2008;103:093542.
[22] Long YW, Yang LX, Yu Y, Li FY, Yu RC, Ding S, et al. High-pressure Raman scattering and structural phase transition in $YCrO_4$. Phys Rev B 2006;74: 054110.
[23] White TJ, ZhiLi D. Structural derivation and crystal chemistry of apatites. Acta Cryst B 2002;59:1–16.
[24] Long YW, Zhang WW, Yang LX, Yu Y, Yu RC, Ding S, et al. Pressure-induced structural phase transition in $CaCrO_4$: evidence from Raman scattering studies. Appl Phys Lett 2005;87:181901.
[25] Pope SJA, West YD. Comparison of the FT Raman spectra of inorganic tetrahedral ions over the temperature range 77 to 473 K. Spectrochim Acta A 1995; 51:2027–37.
[26] Lutz HD, Muller B, Steiner HJ. Lattice vibration spectra. LIX. Single crystal infrared and Raman studies of spinel type oxides. J. Solid State Chem. 1991; 90:54–60.
[27] Kushwaha AK. Studies of interatomic interactions in chromite spinel $CoCr_2O_4$. Chin J Phys 2009;47:355–60.
[28] Luxon JT, Montgomery DJ, Summitt R. Effect of particle size and shape on the infrared absorption of magnesium oxide powders. Phys Rev 1969;188: 1345–56.
[29] Koepke C, Wisniewski K, Grinberg M. Excited state spectroscopy of chromium ions in various valence states in glasses. J Alloys Compd 2002;341: 19–27.
[30] Kim YS, Kim CD, Kim WT. Optical absorption of Co^{2+} ions with S_4 symmetry in $CdGa_2S_4$:Co^{2+}. J Korean Phys Soc 2002;40:952–5.
[31] Oh SK, Song HJ, Kim WT, Kim HG, Lee CI, Park TY, et al. Impurity optical absorption of Co^{2+}-doped $MgAl_2Se_4$ and $CaAl_2Se_4$ single crystals. Semicond Sci Technol 2000;15:108–11.